Optica Applicata, Vol. LIV, No. 3, 2024
DOI: 10.37190/oa240311

Energy flow redistributions of azimuthally polarized Bessel–Gaussian beam modulated by phase plate in tight focusing system

Zijie Zhou[1], Jinsong Li[1,*], Guojin Feng[2,*], Chenxu Lu[1], Shuo Li[1]

[1]China Jiliang University, College of Optics and Electronic, Hangzhou 310018, P.R. China

[2]National Institute of Metrology, Beijing 10029, P.R. China

[*]Corresponding author: lijinsong@cjlu.edu.cn, fengguojin@nim.ac.cn

In this article, we investigate the energy flow redistributions of azimuthally polarized Bessel –Gaussian beams in the focal field by modulating the phase of the phase plate and the topological charge of the phase plate. The results indicate that an increase in phase change parameter will cause the energy flow distribution to shift towards the positive direction of the coordinate axis and result in energy flow separating, while an increase in m will gradually concentrate energy into the center area of the energy flow. The change in phase distribution will affect the shape of energy flow distribution and rotating the phase plate will also bring about changes in the energy flow distribution. These phenomena may contribute to particle capture and transport.

Keywords: energy flow, phase modulation, vortex, tight focusing.

1. Introduction

The study of energy flow distribution has attracted the attention of many researchers, Bekshaev provided a detailed explanation of the phenomenon of internal energy redistribution in light beams [1]. And an increasing number of researchers have conducted research on the energy flow distribution of different beams [2-9]. Jiao *et al*., studied the influence of sector shaped obstacles on the transverse energy flow distribution of diagonally polarized light and utilized sector shaped obstacles to change the partial polarization state of the focal field [10]. Deng *et al*., studied the energy flow and angular momentum distributions of Airy beams under different conditions and found that dimensionless perturbation parameters have an impact on Airy beams [11]. Wang *et al*. used a coupling mode of mixed phase and Gaussian amplitude array to change the energy flow distribution of the Airy beam [12]. Man *et al*. studied the energy flow distributions of azimuthally polarized beam and radially polarized beam separately by changing the phase mask method [13,14]. Li *et al*. studied obtaining continuous negative energy flow by adjusting the polarization distribution of the input beam [15]. Gong used off

axis vortices to disrupt the symmetry of the focal field and multiple vortices to achieve polygonal energy flow distribution [16]. KHONINA can reconstruct the energy flow distribution by changing the characteristics of the vortex beam [17]. GAO *et al*. studied the effect of different phase masks on the redistribution of energy flow in the focal field [18]. However, currently there is limited research on angle polarized Bessel–Gaussian beams with variable phase modulation.

In this article, the energy flow redistributions in the focal field of an azimuthally polarized Bessel–Gaussian beam modulated by phase plate will be discussed, including changing the phase change parameter, the topological charge of the phase plate and numerical aperture (NA) of this focusing system.

2. Theory

As shown in Fig. 1, an azimuthally polarized Bessel–Gaussian beam is modulated by a phase plate and then focused by objective lens.

The structure of the phase plate is shown in Fig. 2, which provides different phase only on the right half of the phase plate. One effective method for modifying the phase of each zone is using a spatial light modulator (SLM). This approach is seen more cap-

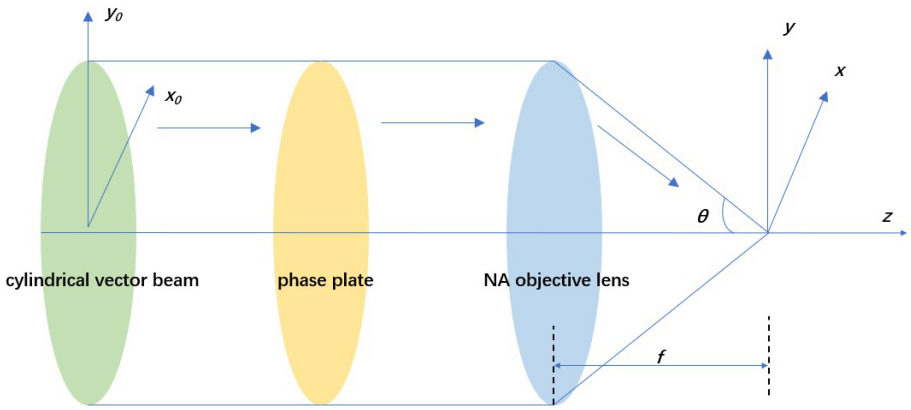

Fig. 1. Schematic of the studied system.

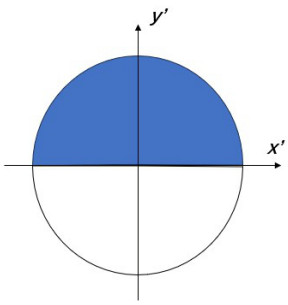

Fig. 2. Structure of the phase plate.

tivating and widely embraced due to its inherent capability of offering dynamic and programmable modulations.

The incident beam is an azimuthally polarized Bessel–Gaussian beam and it can be represented as

$$\mathbf{E}(\theta) = A\exp\left[-\beta^2\left(\frac{\sin\theta}{\sin\alpha}\right)^2\right] J_1\left(2\beta\frac{\sin\theta}{\sin\alpha}\right)\mathbf{e}_\varphi \tag{1}$$

where θ is the convergence angle, and $\theta \in [0, \arcsin(\mathrm{NA})]$. NA is the numerical aperture of this focusing system and A is the amplitude constant. J_1 is the first order Bessel function of the first kind. The maximum convergence angle is α and the waist of the beam is β.

The variant phase of the phase plate can be written as:

$$\phi(\theta, \varphi) = \begin{cases} (D\tan\theta\sin\varphi + 1)\pi, & y' > 0 \\ 0, & y' < 0 \end{cases} \tag{2}$$

where φ is the azimuthal angle. (x', y') and (θ, φ) are the Cartesian and equivalent polar coordinates over the pupil, respectively. D is the phase change parameter.

Based on the vector diffraction theory [19,20], the electric field distribution in the focal region can be written as:

$$E(\rho, \psi, z) = A\iint_{\Omega} E(\theta)\left[(-\sin\varphi)x + (\cos\varphi)y + 0\cdot z\right]\sin\theta\sqrt{\cos\theta}\,\exp(i\phi) \times \exp(im\varphi)\exp\left[-ik\rho\sin\theta\cos(\varphi - \psi)\right]\exp(-ikz\cos\theta)\,\mathrm{d}\theta\,\mathrm{d}\varphi \tag{3}$$

where $k = 2\pi/\lambda$ is called wave number. λ is the wavelength of the incident beam and m denotes the topological charge of the phase plate.

The magnetic field distribution in the focal region can be represented as:

$$\mathbf{H} = \mathbf{k}_0 \times \mathbf{E} \tag{4}$$

where the unit vector of the wave vector is denoted as $\mathbf{k}_0$ and it can be written as:

$$\mathbf{k}_0 = (-\sin\theta\cos\varphi,\ -\sin\theta\sin\varphi,\ \cos\theta) \tag{5}$$

So the Poynting vector can be represented as [20,21]:

$$\mathbf{S} = \frac{c}{8\pi}\mathrm{Re}[\mathbf{E} \times \mathbf{H}^*] \tag{6}$$

3. Numerical results

The distributions of the energy flow at focal plane under different phase and different numerical aperture are simulated in accordance with the formula above. In this article,

the parameters are selected as follows: the waist of the beam $\beta = 1.5$, and the wavelength $\lambda = 632.8$ nm.

First of all, under the condition of NA = 0.8 and $m = 0$, Fig. 3 illustrates the transverse energy flow distribution by modulating D. When $D = 0$, the energy flow distribution is divided into two parts, and most of the energy is concentrated in the two crescent shaped regions (Fig. 3(a)). The energy flow in the left half is counterclockwise, while the energy flow in the right half is clockwise. When D increases from 0 to 1, the energy flow distribution becomes a whole and shows an elliptical distribution (Fig. 3(b)) and the energy flow is counterclockwise. When D continues to increase to 3, the shape of the energy flow distribution undergoes a significant change, exhibiting a distribution of upper and lower parts (Fig. 3(c)). When $D = 5$, the energy flow distribution continues to move in the positive direction of the y-axis, and the energy is mainly concentrated in the lower half (Fig. 3(d)). It is worth noting that in these cases, the energy flow is composed of two clockwise flow rings and one counterclockwise flow ring (Fig. 3(c)-(d)). Overall, as D increases, the energy flow distribution gradually shifts towards the positive y-axis and eventually separates into two parts, with the shape of the energy flow distribution undergoing significant changes. In addition, it can be seen that compared with the energy flow distribution presented in two parts when only phase delay π is added, the energy flow distribution shown in Fig. 3 gradually separates into two parts from a whole at the beginning with the increase of D [17].

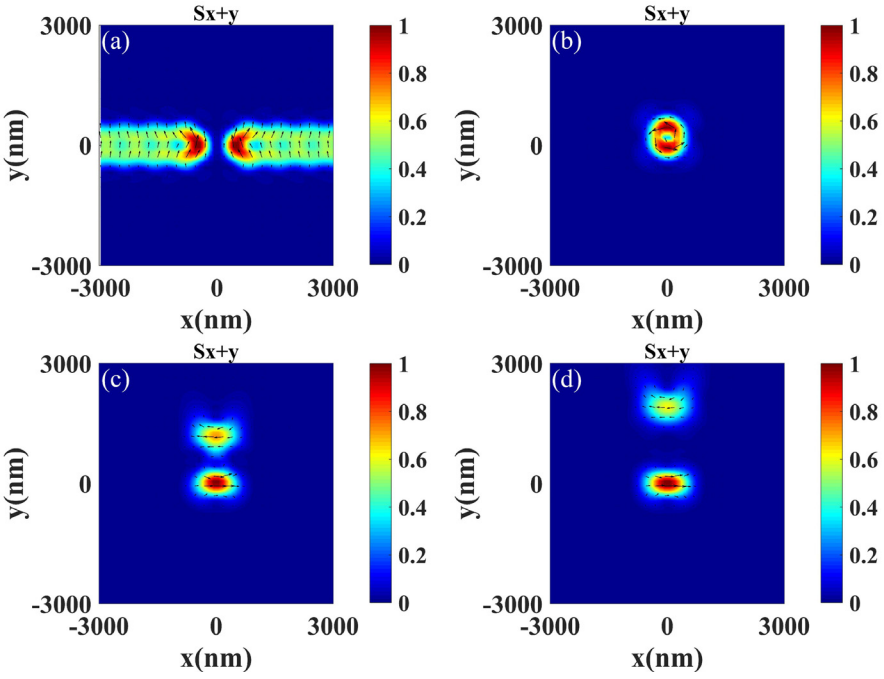

Fig. 3. Transverse energy flow distribution by modulating D. (For explanation, see the text.)

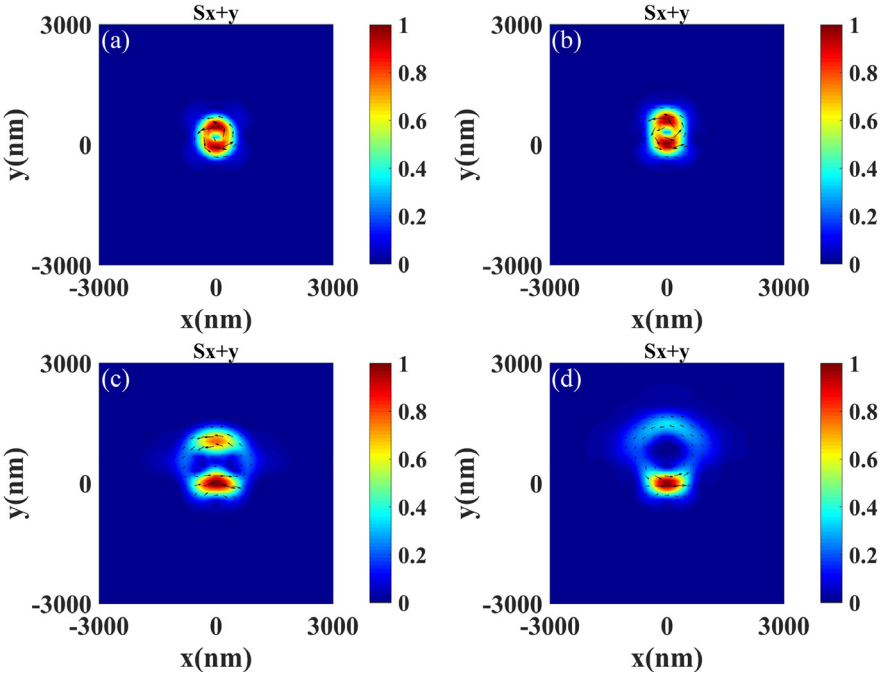

Fig. 4. Transverse energy flow distribution by modulating m. (For explanation, see the text.)

In order to further investigate the influence of vortices on energy flow distribution, we change the value of topological charge m. Under the condition of NA = 0.8 and D = 1, Fig. 4 illustrates the transverse energy flow distribution by modulating m. When m = 0, the energy flow distribution exhibits an elliptical distribution (Fig. 4(a)). When m = 1, the energy flow distribution moves in the positive y-axis direction (Fig. 4(b)). When m = 3, the energy flow distribution consists of two parts: upper and lower, and the energy is mainly concentrated in the lower part (Fig. 4(c)). When m = 5, the energy continues to converge in the lower part (Fig. 4(d)). In Fig. 4, the energy flow is counter-clockwise. In summary, as the topological charge number m increases, energy also gradually concentrates in the central region. By comparing Fig. 3 and Fig. 4, it can be observed that an increase in the phase change rate D and an increase in the topological charge number m will both gradually converge the energy.

In order to further investigate the influence of different NA on the energy flow distribution, we fix the value of D and m. Under the condition of D = 5 and m = 0, Fig. 5 illustrates the transverse energy flow distribution by modulating NA. When NA = 0.7, the upper energy flow density is small, and energy is mainly concentrated in the central region (Fig. 5(a)). When NA = 0.75, the range of energy flow distribution becomes smaller (Fig. 5(b)). As NA continues to increase to 0.8, the density of the upper energy flow decreases (Fig. 5(c)). As NA increases, the density of the energy flow on the upper part continues to decrease and the energy in the central area gradually concentrates

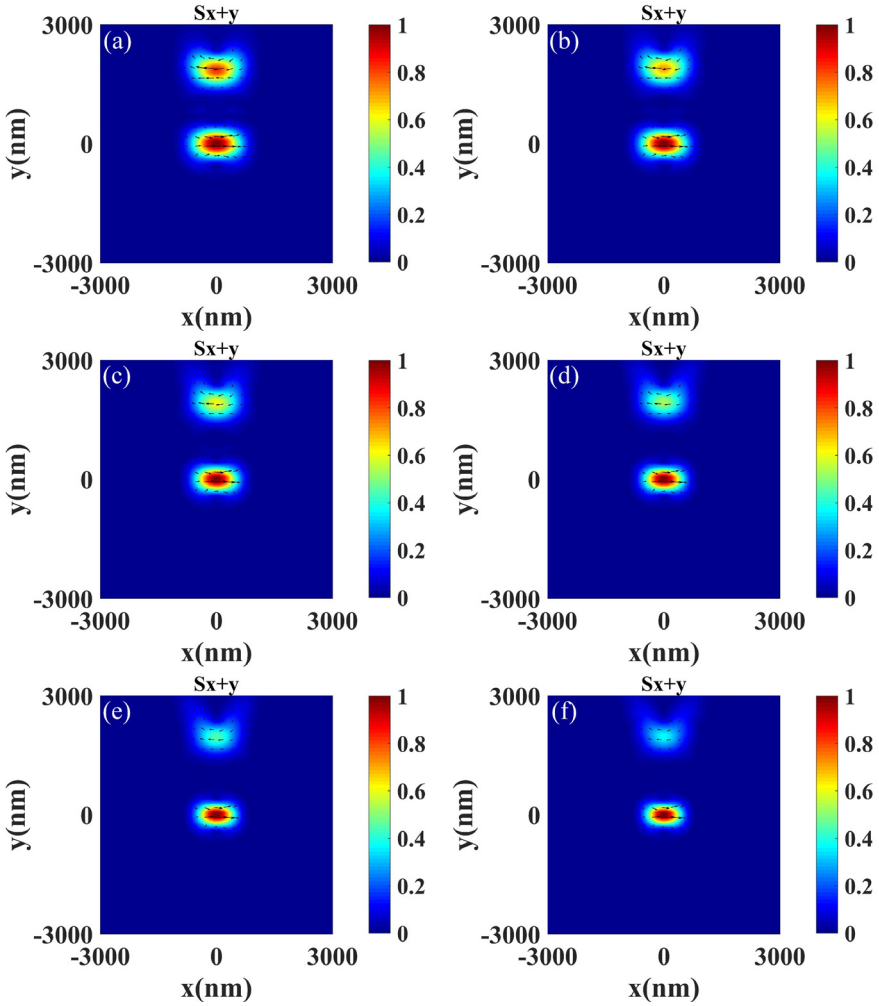

Fig. 5. Transverse energy flow distribution by modulating NA. (For explanation, see the text.)

(Fig. 5(d)-(f)). Overall, as NA increases, the range of energy flow distribution gradually becomes smaller, which also means that the energy flow density decreases at the edge and energy gradually converges to the center area of energy flow distribution. In Fig. 5, the energy flow is composed of one counterclockwise flow ring and two clockwise flow rings. In addition, different from that of ordinary vortex phase modulation, the energy flow exhibits a circular distribution.

For the purpose of better understanding the role of phase plate, we change the phase of the phase plate:

$$\phi(\theta, \varphi) = \begin{cases} (D\tan\theta\sin\varphi)\pi, & y' > 0 \\ 0, & y' < 0 \end{cases} \tag{7}$$

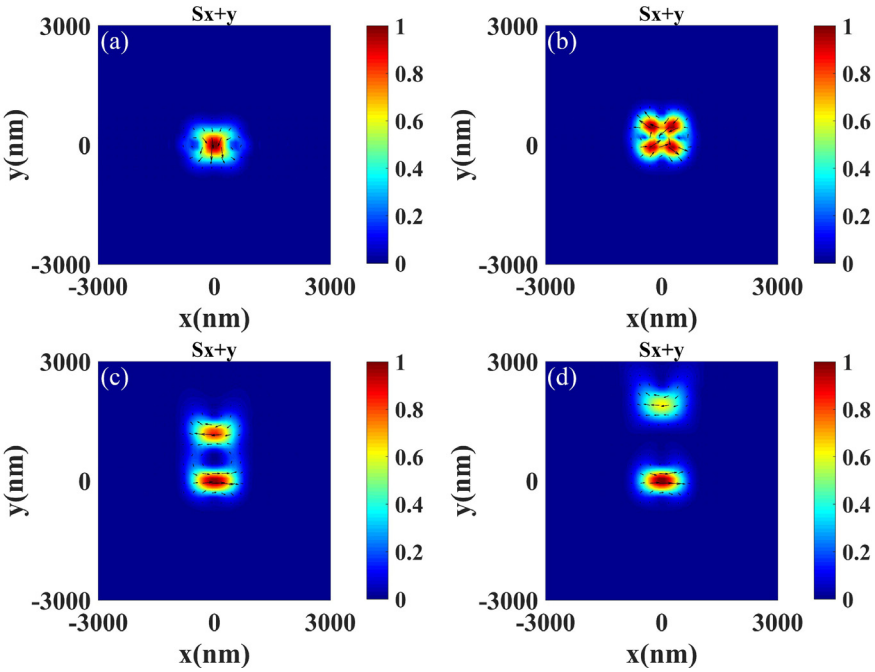

Fig. 6. Transverse energy flow distribution by modulating D. (For explanation, see the text.)

Under the condition of NA = 0.8 and m = 0, Fig. 6 illustrates the transverse energy flow distribution by modulating D. When D = 0, it can be seen that the peak area still appears in the central area. And the energy flow in the left half is clockwise, while the energy flow in the right half is counterclockwise (Fig. 6(a)). When D = 1, the energy flow distribution is in the shape of a four-bladed ventilator and the energy flow direction is composed of two clockwise flow rings and two counterclockwise flow rings (Fig. 6(b)). When D = 3, the energy flow distribution consists of two parts: the upper and the lower parts, with the energy mainly concentrated in the lower part (Fig. 6(c)). When D = 5, the upper part of the energy flow distribution moves towards the positive direction of the y-axis and gradually moves away from the lower part (Fig. 6(d)). At the same time, the energy continues to converge in the lower part. In Fig. 6(c) and (d), the energy flow is composed of two clockwise flow rings and one counterclockwise flow ring.

Under the condition of NA = 0.8 and D = 1, Fig. 7 illustrates the transverse energy flow distribution by modulating m. When m = 0, the energy flow distribution is in the shape of a four-bladed ventilator and the energy flow direction is composed of two clockwise flow rings and two counterclockwise flow rings (Fig. 7(a)). When m = 1, energy tends to gradually accumulate (Fig. 7(a)). When m = 3, the energy flow exhibits a circular distribution, and the energy is mainly concentrated in the lower half of the ring (Fig. 7(c)). When m = 5, the energy tends to further converge (Fig. 7(d)). In

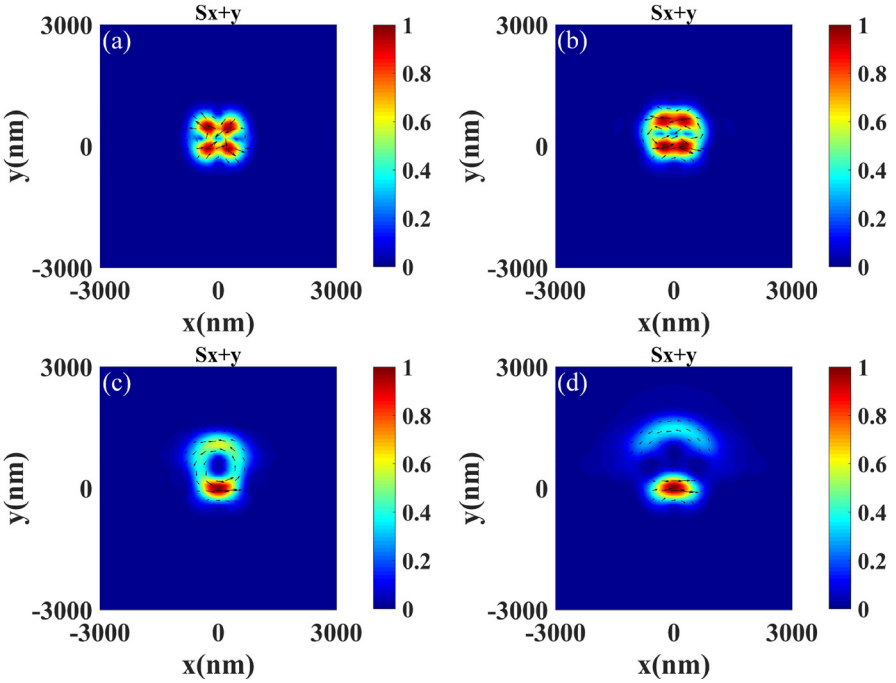

Fig. 7. Transverse energy flow distribution by modulating m. (For explanation, see the text.)

Fig. 7(c) and (d), the energy flow is composed of one clockwise flow ring and one counterclockwise flow ring. Comparing Fig. 6 and Fig. 7, it can also be observed that an increase in phase change rate D and an increase in topological charge number m will gradually converge the energy.

In order to further investigate the variation of energy flow distribution along the x-axis, we change the phase of the phase plate and it can be written as:

$$\phi(\theta, \varphi) = \begin{cases} (D\tan\theta\cos\varphi)\pi, & y' > 0 \\ 0, & y' < 0 \end{cases} \tag{8}$$

Under the condition of NA = 0.8, Fig. 8 illustrates the transverse energy flow distribution by modulating D in Eq. (8). When $D = 0$, the energy flow distribution showed in Fig. 8(a) is the same as Fig. 6(a). When $D = 1$, the energy flow distribution is dumbbell shaped (Fig. 8(b)). When D rises to 3, the energy flow distribution is divided into two parts: left and right, and the density of the energy flow on the right part of the energy flow distribution decreases and moves towards the positive x-axis direction (Fig. 8(c)). When $D = 5$, the distance between the left part and the right part of the energy flow distribution continues to increase and the energy gradually concentrates to the central

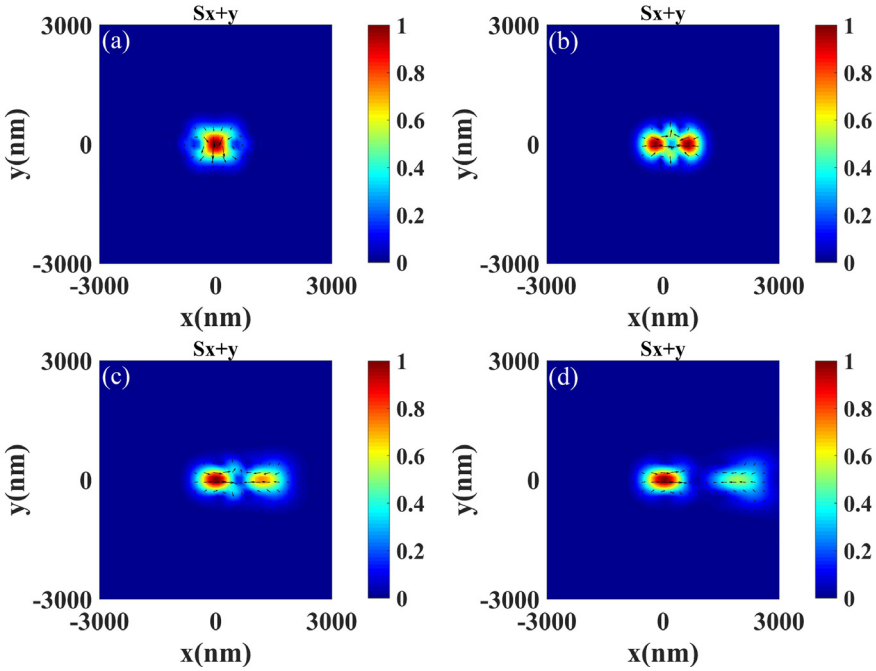

Fig. 8. Transverse energy flow distribution by modulating D. (For explanation, see the text.)

area of energy flow (Fig. 8(d)). In Fig. 8(b)-(d), the energy flow is composed of two counterclockwise flow rings and two clockwise flow rings.

Finally, we change the range of phase distribution on the phase plate to study the changes in energy flow distribution. The first row of Fig. 9 shows four different phase masks. The second row shows four energy flow distributions when NA = 0.8, $m = 0$, and $D = 0$, the third row shows four energy flow distributions when NA = 0.8, $m = 0$, and $D = 1$, the fourth row shows four energy flow distributions when NA = 0.8, $m = 0$, and $D = 3$, and the fifth row shows four energy flow distributions when NA = 0.8, $m = 0$, and $D = 5$. Figure 9(a1)-(a4) have been analyzed in Fig. 3. Comparing Fig. 9(b1) with Fig. 9(a1), it can be observed that after rotating Fig. 9(a1) counterclockwise by 90°, Fig. 9(b1) can be obtained, and the number and direction of energy flow rings remain unchanged. When $D = 1$, as shown in Fig. 9(b2), the energy flow distribution consists of upper and lower parts, which is significantly different from Fig. 9(a2). As D gradually increases to 5, the energy also tends to gradually converge to the central part. It is worth noting that unlike Fig. 9(a2)-(a4), the energy flow in Fig. 9(b2)-(b4) consists of two clockwise and two counterclockwise rings. Next, we also found that in the case of a centrally symmetric phase mask, Fig. 9(c1)-(c4) and Fig. 9(a1)-(a4), Fig. 9(b1)-(b4) and Fig. 9(d1)-(d4) have the same energy flow distribution, respectively.

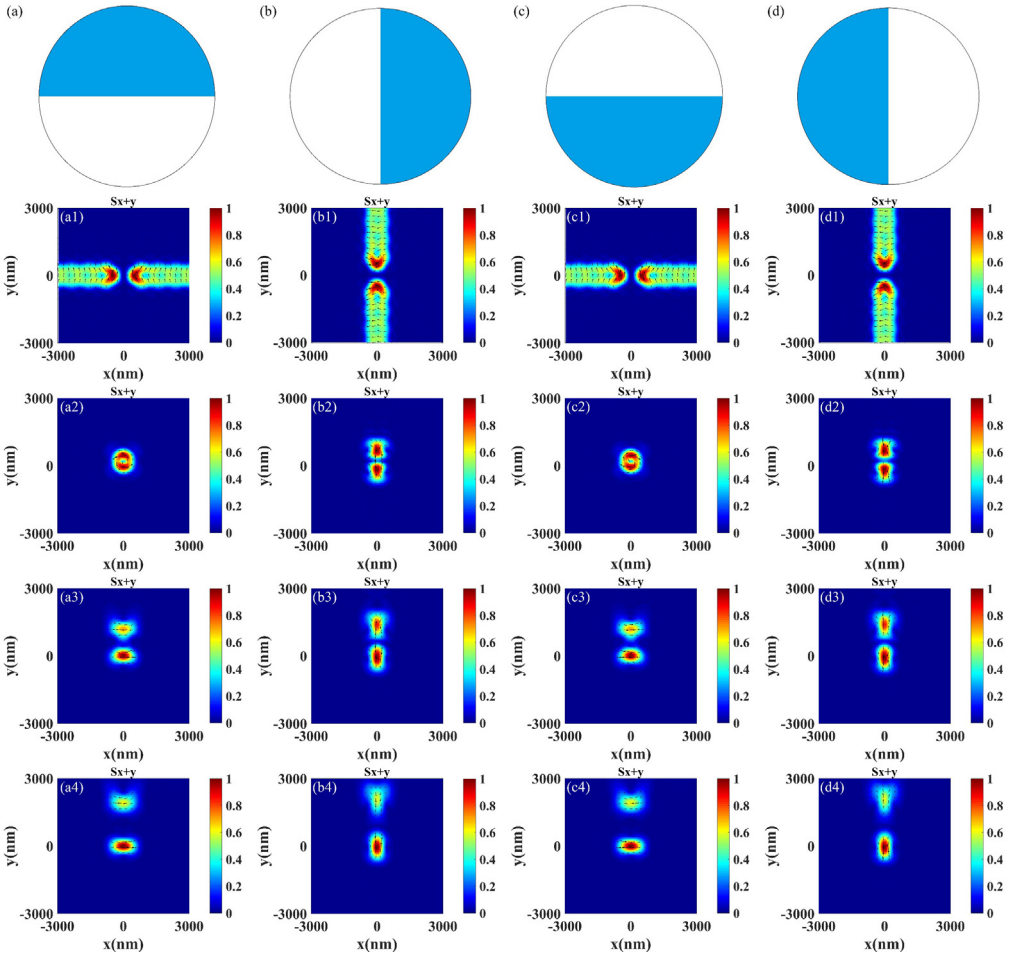

Fig. 9. Changes in energy flow distribution depending on the phase distribution on the phase plate. (For explanation, see the text.)

4. Conclusions

This article investigates the energy flow redistributions of azimuthally polarized Bessel –Gaussian beams in the focal field by changing the phase of a phase plate, the topological charge of the phase plate and NA. Firstly, we investigate the effect of phase change parameter on the energy flow distribution: when the azimuthal phase distribution is sinusoidal, the energy flow distribution gradually moves towards the positive y-axis direction with the increase of D and gradually separates into two parts. When the azimuthal phase distribution is cosine, the energy flow distribution gradually moves towards the positive x-axis direction with the increase of D and tends to separate into two parts. Secondly, we investigate the effect of NA on the energy flow distribution: the range of energy flow distribution gradually becomes smaller with the increase

of NA, and energy gradually converges to the center area of energy flow. Thirdly, when adding vortex phase modulation to the phase plate, the energy also shows a trend of gradually concentrating with the increase of topological charge m. Finally, when the phase plate is rotated, the energy flow distribution also changes. It is worth mentioning that when the two phase plates are symmetrically centered, their energy flow distribution is the same. In addition, the change in phase distribution will affect the shape of energy flow distribution. Overall, these unique distributions may be helpful for particle capture and transport.

Acknowledgements
This work was supported by the Ministry of Science and Technology of the People's Republic of China (2021YFF0600204).

References

[1] Bekshaev A., Bliokh K.Y., Soskin M., *Internal flows and energy circulation in light beams*, Journal of Optics **13**(5), 2011: 053001. https://doi.org/10.1088/2040-8978/13/5/053001
[2] Kotlyar V.V., Kovalev A.A., Nalimov A.G., *Energy density and energy flux in the focus of an optical vortex: Reverse flux of light energy*, Optics Letters **43**(12), 2018: 2921-2924. https://doi.org/10.1364/OL.43.002921
[3] Kotlyar V.V., Nalimov A.G., Stafeev S.S., *Exploiting the circular polarization of light to obtain a spiral energy flow at the subwavelength focus*, Journal of the Optical Society of America B **36**(10), 2019: 2850-2855. https://doi.org/10.1364/JOSAB.36.002850
[4] Wu G., Wang F., Cai Y., *Generation and self-healing of a radially polarized Bessel-Gauss beam*, Physical Review A **89**(4), 2014: 043807. https://doi.org/10.1103/PhysRevA.89.043807
[5] Yuan W., Man Z., *Manipulating the magnetic energy density and energy flux by cylindrically symmetric state of polarization*, Optik **185**, 2019: 208-214. https://doi.org/10.1016/j.ijleo.2019.03.103
[6] Zannotti A., Vasiljević J.M., Timotijević D.V., Jović Savić D.M., Denz C., *Visualizing the energy flow of Tailored ligh*, Advanced Optical Materials **6**(8), 2018: 1701355. https://doi.org/10.1002/adom.201701355
[7] Man Z., Dou X., Urbach H.P., *The evolutions of spin density and energy flux of strongly focused standard full Poincaré beams*, Optics Communications **458**, 2020: 124790. https://doi.org/10.1016/j.optcom.2019.124790
[8] Yuan G.H., Wei S.B., Yuan X.-C., *Generation of nondiffracting quasi-circular polarization beams using an amplitude modulated phase hologram*, Journal of the Optical Society of America A **28**(8), 2011: 1716-1720. https://doi.org/10.1364/JOSAA.28.001716
[9] Zhou J, Ma H., Zhang Y., Zhang S., Min C., Yuan X., *Energy flow inversion in an intensity-invariant focusing field*, Optics Letters **47**(6), 2022: 1494-1497. https://doi.org/10.1364/OL.449056
[10] Jiao X., Liu S., Wang Q., Gan X., Li P., Zhao J., *Redistributing energy flow and polarization of a focused azimuthally polarized beam with rotationally symmetric sector-shaped obstacles*, Optics Letters **37**(6), 2012: 1041-1043. https://doi.org/10.1364/OL.37.001041
[11] Deng D., Du S., Guo Q., *Energy flow and angular momentum density of nonparaxial Airy beams*, Optics Communications **289**, 2013: 6-9. https://doi.org/10.1016/j.optcom.2012.09.007
[12] Wang G., Yu D., Miao Y., Li Z., Shan X., Gao X., *An active energy compensation method of 2D Airy beam*, Optik **225**, 2021: 165805. https://doi.org/10.1016/j.ijleo.2020.165805
[13] Man Z., Li X., Zhang S., Bai Z., Lyu Y., Li J., Ge X., Sun Y., Fu S., *Manipulation of the transverse energy flow of azimuthally polarized beam in tight focusing system*, Optics Communications **431**, 2019: 174-180. https://doi.org/10.1016/j.optcom.2018.09.028

[14] MAN Z., BAI Z., ZHANG S., LI X., LI J., GE X., ZHANG Y., FU S., *Redistributing the energy flow of a tightly focused radially polarized optical field by designing phase masks*, Optics Express **26**(18), 2018: 23935-23944. https://doi.org/10.1364/OE.26.023935

[15] LI H., WANG C., TANG M., LI X., *Controlled negative energy flow in the focus of a radial polarized optical beam*, Optics Express **28**(13), 2020: 18607-18615. https://doi.org/10.1364/OE.391398

[16] GONG L., WANG X., ZHU Z., LAI S., FENG H., WANG J., GU B., *Transversal energy flow of tightly focused off-axis circular polarized vortex beams*, Applied Optics **61**(17), 2022: 5076-5082. https://doi.org/10.1364/AO.459816

[17] KHONINA S.N., PORFIREV A.P., USTINOV A.V., BUTT M.A., *Generation of complex transverse energy flow distributions with autofocusing optical vortex beams*, Micromachines **12**(3), 2021: 297. https://doi.org/10.3390/mi12030297

[18] GAO X.-Z., PAN Y., ZHANG G.-L., ZHAO M.-D., REN Z.-C., TU C.-G., LI Y.-N., WANG H.-T., *Redistributing the energy flow of tightly focused ellipticity-variant vector optical fields*, Photonics Research **5**(6), 2017: 640-648. https://doi.org/10.1364/PRJ.5.000640

[19] WOLF E., *Electromagnetic diffraction in optical systems. I. An integral representation of the image field*, Proceedings of the Royal Society of London **253**(1274), 1959: 349-357. https://doi.org/10.1098/rspa.1959.0199

[20] RICHARDS B., WOLF E., *Electromagnetic diffraction in optical systems. II. Structure of the image field in an aplanatic system*, Proceedings of the Royal Society of London **253**(1274), 1959: 358-379. https://doi.org/10.1098/rspa.1959.0200

[21] WANG H., SHI L., LUKYANCHUK B., SHEPPARD C., CHONG C.T., *Creation of a needle of longitudinally polarized light in vacuum using binary optics*, Nature Photonics **2**, 2008: 501-505. https://doi.org/10.1038/nphoton.2008.127

Received April 9, 2024
in revised form June 18, 2024